

Comprehensive analysis of large α -yields in ${}^6\text{Li}$ induced reactions

Jin Lei^{1,*} and Antonio M. Moro^{1,†}

¹*Departamento de FAMN, Universidad de Sevilla, Apartado 1065, 41080 Sevilla, Spain.*

(Dated: December 13, 2024)

Background: Large α yields have been reported over the years in reactions with ${}^6\text{Li}$ and ${}^7\text{Li}$ projectiles. Previous theoretical analyses have shown that the elastic breakup (EBU) mechanism (i.e., projectile breakup leaving the target in its ground state) is able to account only for a small fraction of the total α inclusive breakup cross sections, pointing toward the dominance of non-elastic breakup (NEB) mechanisms.

Purpose: We aim to provide a systematic study of the α inclusive cross sections observed in nuclear reactions induced by ${}^6\text{Li}$ projectiles. In addition to estimating the total α singles cross sections, it is our goal to evaluate angular and energy distributions of these α particles and compare with experimental data, when available.

Method: We compute separately the EBU and NEB components of the inclusive breakup cross sections. For the former, we use the continuum-discretized coupled-channels (CDCC) method, which treats this mechanism to all orders. For the NEB part, we employ the model proposed in the eighties by Ichimura, Austern and Vincent [Phys. Rev. C32, 432 (1982)], within the DWBA approximation.

Results: Overall, the sum of the computed EBU and NEB cross sections is found to reproduce very well the measured singles cross sections. In all cases analyzed, we find that the inclusive breakup cross section is largely dominated by the NEB component.

Conclusions: The presented method provides a global and systematic description of inclusive breakup reactions induced by ${}^6\text{Li}$ projectiles. It provides also a natural explanation of the previously observed underestimation of the measured α yields by CDCC calculations. The method used here can be extended to other weakly-bound nuclei, including halo nuclei.

I. INTRODUCTION

Reactions induced by the ${}^6\text{Li}$ nucleus have been extensively studied giving rise to a large body of experimental data at present. Given its marked $\alpha + d$ structure, with a separation energy of 1.474 MeV (to be compared with the single nucleon separation energy of 5.39 MeV), one may anticipate that the breakup of this nucleus into α and d is a major reaction channel. In fact, experimental data show remarkably large yields of α particles but, contrary to what naively expected, these yields are typically much larger than the corresponding d yields. This suggests that the breakup of the ${}^6\text{Li}$ is not a simple direct breakup mechanism.

From the theoretical point of view, a proper interpretation of these α yields is still lacking. Continuum-discretized coupled-channels (CDCC) calculations, which treat the ${}^6\text{Li}$ breakup as an inelastic excitation to the continuum, reproduce successfully the coincidence $\alpha + d$ measurements [1] but they largely underestimate the inclusive α cross sections. It is worthwhile recalling that the CDCC method provides only the so-called *elastic breakup* (EBU) component of the total breakup cross section. For the reaction of a ${}^6\text{Li}$ projectile impinging on a target A , this corresponds to the processes of the form ${}^6\text{Li} + A \rightarrow \alpha + d + A_{\text{g.s.}}$ in which the two-projectile clusters survive after the collision and the target remains in

the ground state.¹ Thus, the underestimation of the inclusive α yields by the CDCC calculations means that there other mechanisms contributing to the inclusive breakup cross section other than the EBU. These include the exchange of nucleons between d and A , the projectile dissociation accompanied by target excitation, and the fusion of d by A , among others, that we will globally denote as *non-elastic breakup* (NEB) channels. An explicit account of these process is very challenging due to the huge number of accessible final states and the variety of competing different mechanisms.

When one is only interested in the evaluation of the singles cross section (for example, the energy or angular distribution of α particles), rather than on the separate contributing mechanisms, one may resort to the inclusive breakup models proposed in the 1980s and recently reexamined by several groups [2–6]. In these models, the sum over all the possible final states through which the unobserved fragment d may interact with the target is done in a formal way, making use of the Feshbach projection formalism [7] and closure.

In this work, we will show that inclusive α singles cross sections from ${}^6\text{Li}$ -induced reactions can be remarkably well reproduced using the inclusive breakup model proposed by Ichimura, Austern and Vincent (IAV) [8]. To our knowledge, this is the first study of this kind providing a systematic explanation of these data.

* jinlei@us.es; Present address: Institute of Nuclear and Particle Physics, and Department of Physics and Astronomy, Ohio University, Athens, Ohio 45701, USA

† moro@us.es

¹ If a three-body description of the ${}^6\text{Li}$ is used, $\alpha + p + n$, the three-body breakup mode ${}^6\text{Li} + A \rightarrow \alpha + p + n + A_{\text{g.s.}}$ would be also part of the elastic breakup channel. Since we resort here to a two-body model of ${}^6\text{Li}$ we include this channel in the NEB part.

Although the IAV model provides a common formalism for the calculation of the elastic and non-elastic breakup components of the inclusive breakup cross section, in our analysis we will employ this model only for the NEB part, whereas for the EBU part we will use the continuum-discretized coupled-channels (CDCC) method, which treats breakup to all orders.

The paper is organized as follows. In Sec. II we give a short overview of the IAV theory, highlighting only its main formulas. In Sec. III the extension of the formalism to negative deuteron energies (bound states) is discussed. In Sec. IV, the formalism is applied to describe the α cross sections in several ${}^6\text{Li}$ -induced reactions comparing with the available data. In Sec. V the role of the transfer channels on the NEB cross section is discussed. In Sec. VI we investigate the systematic behaviour of the inclusive cross section with respect to the incident energy and for all analyzed targets. Finally, in Sec. VII we summarize the main results of this work.

II. THE ICHIMURA, AUSTERN, VINCENT (IAV) MODEL

In this section we briefly summarize the model of Ichimura, Austern and Vincent (IAV), whose original derivation can be found in [8, 9], and has been also recently revisited by several authors [2, 3, 5, 6]. We outline here the main results of this model, and refer the reader to these references for further details on their derivations.

We write the process under study in the form,

$$a(=b+x)+A\rightarrow b+B^*. \quad (1)$$

This process will be described with the effective Hamiltonian

$$H = K + V_{bx} + U_b(\vec{r}_b) + H_A(\xi) + V_{xA}(\xi, \vec{r}_x), \quad (2)$$

where K is the total kinetic energy operator, V_{bx} is the interaction binding the two clusters b and x in the initial composite nucleus a , $H_A(\xi)$ is the Hamiltonian of the target nucleus (with ξ denoting its internal coordinates) and V_{xA} and U_b are the fragment-target interactions. The relevant coordinates are depicted in Fig. 1.

In writing the Hamiltonian of the system in the form (2) we make a clear distinction between the two cluster constituents; the interaction of the fragment b , the one that is assumed to be observed in the experiment, is described with a (complex) optical potential. Non-elastic processes arising from this interaction (e.g. target excitation), are included only effectively through U_b . The particle b is said to act as *spectator*. On the other hand, the interaction of the particle x with the target retains the dependence of the target degrees of freedom (ξ).

Starting from Hamiltonian (2) IAV derived the following expression for the double differential cross section for the NEB with respect to the angle and energy of the b

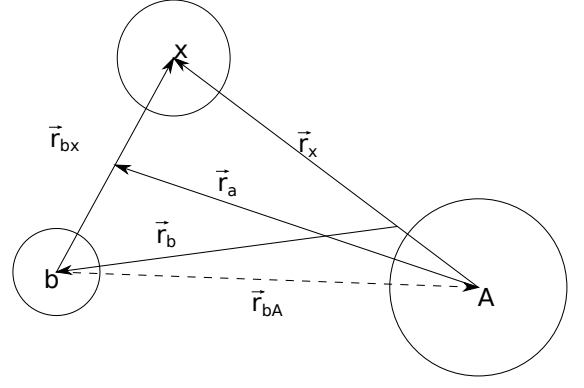


FIG. 1. (Color online) Coordinates used in the non-elastic breakup calculations.

fragments:

$$\left. \frac{d^2\sigma}{dE_b d\Omega_b} \right|_{\text{NEB}} = -\frac{2}{\hbar v_a} \rho_b(E_b) \langle \psi_x^{(0)}(\vec{k}_b, \vec{r}_x) | W_x | \psi_x^{(0)}(\vec{k}_b, \vec{r}_x) \rangle. \quad (3)$$

where v_a is the projectile-target relative velocity, $\rho_b(E_b) = k_b \mu_b / ((2\pi)^3 \hbar^2)$ is the density of states for the particle b , W_x is the imaginary part of the optical potential describing $x + A$ elastic scattering and $\psi_x^{(0)}(\vec{k}_b, \vec{r}_x)$ is the so-called x -channel wave function, which governs the evolution of x after the projectile dissociation, when b scatters with momentum \vec{k}_b and the target remains in the ground state. This function satisfies the following inhomogeneous differential equation

$$(E_x - K_x - U_{xA}) \psi_x^{(0)}(\vec{k}_b, \vec{r}_x) = (\chi_b^{(-)}(\vec{k}_b, \vec{r}_b) | V_{\text{post}} | \Psi^{3b}), \quad (4)$$

where $E_x = E - E_b$, $\chi_b^{(-)}$ is the distorted-wave describing the scattering of b in the final channel with respect to the $x+B$ sub-system, and $V_{\text{post}} \equiv V_{bx} + U_{bA} - U_b$ (with U_b the optical potential in the final channel) is the post-form transition operator. This equation is to be solved with outgoing boundary conditions.

Austern *et al.* [9] suggest approximating the three-body wave function appearing in the source term of Eq. (4), Ψ^{3b} , by the CDCC one. Since the CDCC wave function is also a complicated object by itself, a simpler choice is to use the DWBA approximation, i.e., $\psi_x^{3b} \approx \chi_a^{(+)}(\vec{r}_a) \phi_{bx}(\vec{r}_{bx})$, where $\chi_a^{(+)}$ is a distorted wave describing $a+A$ elastic scattering and ϕ_{bx} is the projectile ground state wave function.

The IAV model has been recently revisited by several groups [2, 5, 6]. All the calculations performed so far by these groups make use of the DWBA approximation for the incoming wave function. In Refs. [5, 6], the theory was applied to deuteron induced reactions of the form $A(d, pX)$, and in Ref. [2] the model was extended to ${}^6\text{Li}$ projectiles, presenting a first application to the ${}^{209}\text{Bi}({}^6\text{Li}, \alpha X)$ reaction. In general, the agreement with the data has been found to be very encouraging, although

further comparisons with experimental data are advisable to better assess the validity and limitations of the model.

III. EXTENSION OF IAV MODEL TO $E_x < 0$

The sort of breakup cross section considered by Ichimura, Austern and Vincent can be regarded as transfer to continuum process populating $x + A$ states with positive relative energy ($E_x > 0$). In general, the inclusive cross section will also contain contributions coming from the population of states below the breakup $x + A$ threshold ($E_x < 0$). For example, in a (${}^6\text{Li}$, αX) reaction, the α 's emitted at the higher energies will actually correspond to deuteron transfer to bound states of the target nucleus. One would like to have a common framework to describe transfer to continuum states as well as to bound states. The explicit inclusion of all possible final bound states is impractical because of their large number and the uncertainties in their spin/parity assignments and spectroscopic factors. An alternative procedure was proposed by Udagawa and co-workers [10]. The key idea is to extend the complex potential to negative energies. Then, the bound states of the system are simulated by the eigenstates in this complex potential. The imaginary part will be associated with the spreading width of the single-particle states, which accounts for the fragmentation of these states into more complicated configurations due to the residual interactions. The method has been recently reexamined by Potel *et al.* [11], who have provided an efficient implementation of this idea. Here, we closely follow their formulation. For that, we first rewrite Eq. (4) in integral form

$$\psi_x^{(0)}(\vec{k}_b, \vec{r}_x) = \int_0^\infty G_x(\vec{r}_x, \vec{r}'_x) \rho(\vec{k}_b, \vec{r}'_x) d^3 r_x, \quad (5)$$

where $\rho(\vec{k}_b, \vec{r}'_x) = (\chi_b^{(-)}(\vec{k}_b) | V_{\text{post}} | \Psi^{3b})$ is the source term of the inhomogeneous Eq. (4) and $G_x(\vec{r}_x, \vec{r}'_x)$ is the Green's function

$$G_x(\vec{r}_x, \vec{r}'_x) = \frac{1}{r_x r'_x} \sum_{l_x m_x} g_{l_x}(r_x, r'_x) Y_{l_x}^{m_x*}(\hat{r}'_x) Y_{l_x}^{m_x}(\hat{r}_x), \quad (6)$$

where $g_{l_x}(r_x, r'_x)$ satisfies the equation

$$(E_x - K_x - U_{xA}) g_{l_x}(r_x, r'_x) = \delta(r_x - r'_x). \quad (7)$$

As usual, the solution of this equation is obtained from the regular ($f_{l_x}(r_x)$) and irregular ($h_{l_x}^{(+)}(r_x)$) solutions of the corresponding homogeneous equation. From these two solutions, $g_{l_x}(r_x, r'_x)$ can be expressed as

$$g_{l_x}(r_x, r'_x) = N_{l_x} f_{l_x}(r_{<}) h_{l_x}^{(+)}(r_{>}), \quad (8)$$

where $r_{<}$ is the lesser value of r_x and r'_x and $r_{>}$ is the larger one. The normalization constant N_{l_x} can be

found by integrating Eq. (7) over an infinitesimal interval around r'_x

$$\begin{aligned} \frac{2\mu_x}{\hbar^2} &= \int_{r'_x - \delta}^{r'_x + \delta} dr_x \frac{d^2}{dr_x^2} g_{l_x}(r_x, r'_x) = \frac{d}{dr_x} g_{l_x}(r_x, r'_x) \Big|_{r'_x - \delta}^{r'_x + \delta} \\ &= N_{l_x} \left[f_{l_x}(r'_x) \frac{d}{dr_x} h_{l_x}^{(+)}(r'_x + \delta) \right. \\ &\quad \left. - h_{l_x}^{(+)}(r'_x) \frac{d}{dr_x} f_{l_x}(r'_x - \delta) \right] \\ &\xrightarrow{\delta \rightarrow 0} N_{l_x} \mathcal{W}[f_{l_x}(r'_x), h_{l_x}^{(+)}(r'_x)] \end{aligned} \quad (9)$$

Where \mathcal{W} denotes a Wronskian, which is independent of the value of r'_x .

It is worth noting that the integral form of the x -channel wave function (5) can be also be used for positive $x - A$ energies. Proceeding in this way, the application of the IAV formalism to positive and negative energies is formally analogous. Despite this formal similitude, the interpretation of the channel function and of the underlying imaginary part of the potential is somewhat different in both regions. For $E_x > 0$ the channel function $\psi_x^{(0)}$ describes $x - A$ elastic scattering and the imaginary part is therefore associated with the flux leaving this channel in favor of non-elastic channels. For $E_x < 0$, the channel wave-function describes the motion of the x particle in a bound single-particle configuration state of the residual nucleus, and the imaginary part is connected with the spreading width of this configuration, which accounts for the fragmentation of these states into more complicated configurations. The connection between both regimes becomes more transparent within a dispersive formulation of the optical potential, as suggested long ago by Mahoux and Sartor [12, 13] and recently reexamined by several groups (see e.g. [14]).

IV. COMPARISON WITH EXPERIMENTAL DATA

In this section, we compare the formalism with existing ${}^6\text{Li}$ inclusive breakup data on different targets. The ${}^6\text{Li}$ nucleus is treated in a two-cluster model ($\alpha + d$), with α and d playing the roles of spectator and participant in the IAV model, respectively.

The elastic breakup (EBU) contribution of the inclusive breakup cross section is evaluated with the CDCC method [9], using the coupled-channels code FRESKO [15]. In this method, the breakup is treated as an inelastic excitation to the continuum states of the projectile. Although four-body CDCC calculations for ${}^6\text{Li}$ scattering have become recently available [16], we rely here on the more conventional $\alpha + d$ di-cluster model. Thus, diagonal and off-diagonal coupling potentials are generated from the d -target and α -target interactions, evaluated at 2/3 and 1/3 of the projectile incident energy, respectively. In

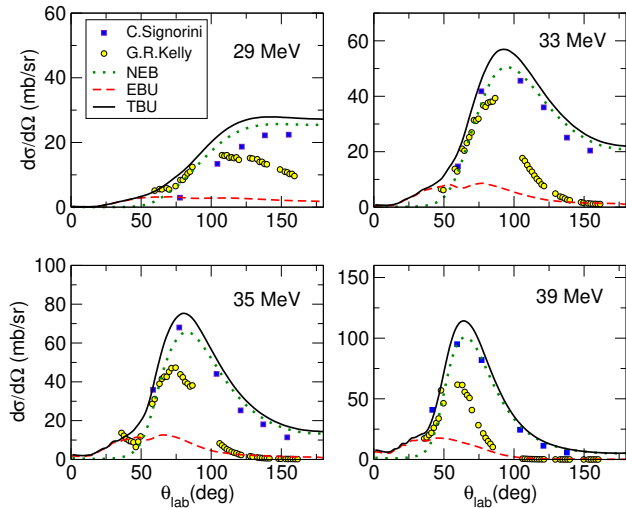


FIG. 2. (Color online) Angular distribution of α particles produced in the reaction ${}^6\text{Li}+{}^{208}\text{Pb}$ at the incident energies indicated by the labels. The dotted, dashed and solid lines correspond to the NEB (IAV model), EBU (CDCC) and their sum, respectively. Experimental data are from Refs. [19, 20]. See text for details.

order to reproduce correctly the elastic scattering data, CDCC calculations based on this two-body model typically require some renormalization of the fragment-target potentials [16, 17]. This has been recently found to be a consequence of the shortcomings of the two-body description of the ${}^6\text{Li}$ nucleus, which results in an effective suppression of the deuteron-target absorption [16]. In our previous work [2], we found that this effect could be well simulated by removing the surface part of the deuteron-target optical potential. In the calculations presented in this work, we also allow for such kind of modification, in order to reproduce correctly the elastic scattering data.

For the $\alpha + d$ potential, we use the potential model from Ref. [18], which contains both central and spin-orbit terms, with the latter required to place correctly the $\ell = 2$ resonances.

For the non-elastic breakup calculations, we rely also on a $\alpha + d$ model, but the spin of the deuteron is ignored, since our current implementation of the IAV model ignores the intrinsic spin of the fragments. This approximation was also used in our previous works [2–4].

A. ${}^{208}\text{Pb}({}^6\text{Li}, \alpha X)$

First, the results for the reaction ${}^{208}\text{Pb}({}^6\text{Li}, \alpha X)$, at several energies between 29 and 39 MeV are presented, comparing with the data from Refs. [19, 20]. The nominal Coulomb barrier for this system is around 29.5 MeV [19]. The CDCC calculations use the same structure model and bin discretization as in our previous calculations for ${}^6\text{Li}+{}^{209}\text{Bi}$ [2]. The $d-{}^{208}\text{Pb}$ and $\alpha-{}^{208}\text{Pb}$ optical potentials are taken from Refs. [21] and [22], respectively. To

improve the reproduction of the elastic data, the surface term of the imaginary part of the $d+{}^{208}\text{Pb}$ potential was removed. For the NEB calculations, the optical potential of ${}^6\text{Li}+{}^{208}\text{Pb}$ is taken from Ref. [23].

Figure 2 shows the comparison of the calculated and experimental angular distributions of α particles produced in this reaction at the measured incident energies. The squares and circles are the experimental data from Refs. [19] and [20], respectively. It is evident that there is an appreciable difference between the two sets of data. The dashed and dotted lines are the EBU (CDCC) and NEB (IAV model in DWBA) results. As in the ${}^6\text{Li}+{}^{209}\text{Bi}$ case [2], the NEB is found to account for most of the inclusive breakup cross section. The sum of EBU and NEB reproduces reasonably well the magnitude and shape of the data of Ref. [19], except for some overestimation for the lowest energies. Thus, our calculations clearly favour the data presented in Ref. [19] over those presented in [20].

From the results shown here and in Ref. [2], it can be concluded that the nonelastic breakup process is the dominant α -emitting channel in the ${}^6\text{Li}$ induced reactions on heavy targets. To investigate whether this conclusion is a general feature of ${}^6\text{Li}$ induced reactions or it holds only for heavy targets we extend our analysis to lighter targets.

B. ${}^{159}\text{Tb}({}^6\text{Li}, \alpha X)$

This reaction has been measured by Pradhan *et al.* [24] at several energies between 23 MeV and 35 MeV.

In Ref. [24], the following processes were invoked to explain the observed α yields: (i) breakup of ${}^6\text{Li}$ into α and d fragments where both fragments escape without being captured by the target, referred to in some works as non-capture breakup; (ii) α particles resulting from d capture by the target (*deuteron incomplete fusion*), following the breakup of ${}^6\text{Li}$ into α and d or a one step transfer to the target; (iii) single-proton stripping from ${}^6\text{Li}$ to produce the unbound ${}^5\text{He}$ nucleus that decays into an α particle and a neutron; (iv) single-neutron stripping from ${}^6\text{Li}$ to produce ${}^5\text{Li}$, which will subsequently decay into an α particle plus a proton; and (v) single-neutron pickup from ${}^6\text{Li}$ to produce ${}^7\text{Li}$, which breaks into an α particle and a triton if ${}^7\text{Li}$ is excited above its breakup threshold of 2.468 MeV. In Ref. [24] these processes were treated separately, using several reaction formalisms and their sum reasonably reproduces the total α -particle cross sections, but not their angular distributions.

Within the inclusive breakup model adopted here, the processes discussed by Pradhan *et al.* [24] can be re-defined as follows: process (i) can be divided into two parts. First, the non-capture breakup with the target remaining in its ground state, i.e., EBU. Second, the non-capture breakup accompanied by target excitation, which we call *inelastic breakup* and is part of our *non-elastic breakup* cross section; processes (ii)-(iv) may be

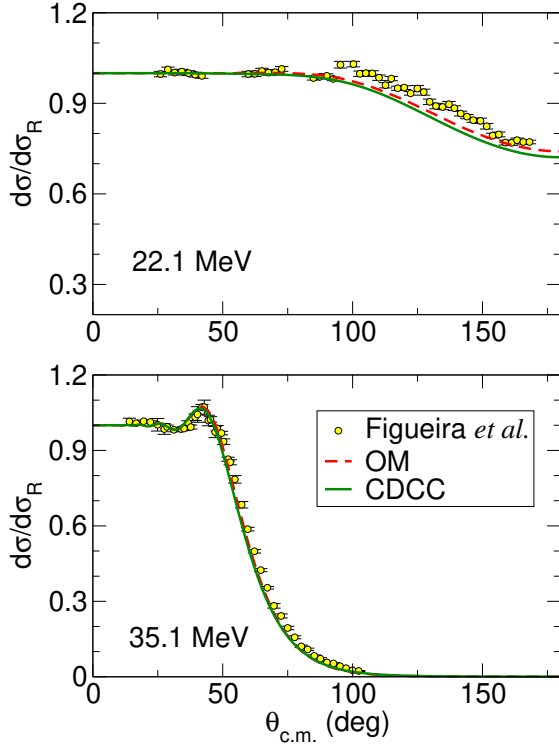


FIG. 3. (Color online) Elastic scattering of ${}^6\text{Li}+{}^{144}\text{Sm}$ at 22.1 MeV (top) and 35.1 MeV (bottom). The solid and dashed lines are, respectively, the CDCC calculation and the optical model calculation with the optical potential from [23]. Experimental data are from Ref. [25].

also embedded in the NEB part, in which the deuteron is absorbed by the target or it breaks up into $p+n$ following the breakup of ${}^6\text{Li}$ into α and d ; it can also happen that after the breakup of ${}^6\text{Li}$, the deuteron picks a neutron to become a tritium, contributing to the process (v). Processes (ii)-(v) as well as the inelastic breakup can be considered as nonelastic breakup and should be therefore accounted by the IAV formalism.

Elastic data for this reaction are not available. Thus, the CDCC calculation is tested against the data for the nearby system ${}^6\text{Li}+{}^{144}\text{Sm}$ [25]. The $\alpha+{}^{144}\text{Sm}$ and $d+{}^{144}\text{Sm}$ optical potentials were taken from Refs. [26] and [21], respectively. The optical model calculation using the potential of Cook [23] (dashed lines) is also shown. It can be seen that the CDCC result is similar to the optical model calculation, particularly at $E = 35.1$ MeV. At this energy, the calculations reproduce very well the elastic data. For the lower energy ($E = 22.1$ MeV), both calculations underestimate the data at backward angles. Note that, in contrast to the ${}^6\text{Li}+{}^{208}\text{Pb}$ case, no apparent modification of the deuteron potential was required in this case.

Now the inclusive breakup cross sections ${}^{159}\text{Tb}({}^6\text{Li}, \alpha X)$ are discussed. The EBU contribution was obtained from the CDCC calculations discussed

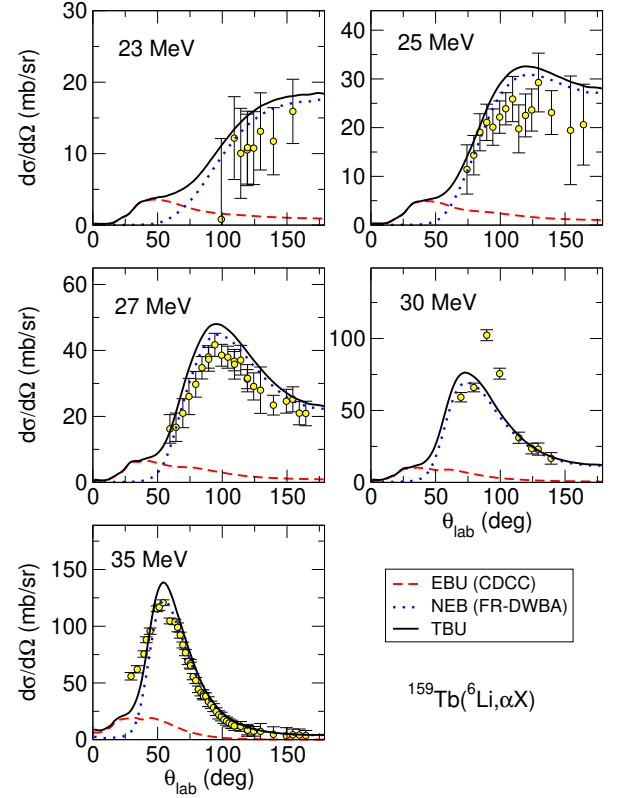


FIG. 4. (Color online) Angular distribution of α particle production of the reaction ${}^6\text{Li}+{}^{159}\text{Tb}$ at the incident energies indicated by the labels. The dashed, dotted and solid lines are EBU calculated with CDCC, NEB calculated with finite-range DWBA and their sum, respectively. The experimental data are taken from Ref. [24].

in the previous paragraph. For the NEB calculation, the same optical potentials $\alpha/d+{}^{159}\text{Tb}$ were used. The Cook potential [23] was used to calculate the distorted wave of the incoming channel.

In Fig. 4 the calculated and experimental angular distributions of α particles are compared for several incident energies of ${}^6\text{Li}$. The dashed and dotted lines are the EBU (CDCC) and NEB (IAV model) results. The summed EBU + NEB cross sections (solid lines) reproduce fairly well the shape and magnitude of the data, except for a slight overestimation at some energies. Similarly to the heavy-target systems, i.e., ${}^6\text{Li}+{}^{209}\text{Bi}$ [2] and ${}^6\text{Li}+{}^{208}\text{Pb}$ (Sec. IV A), the NEB is found to account for most of the inclusive breakup cross section.

C. ${}^{118}\text{Sn}({}^6\text{Li}, \alpha X)$

Inclusive breakup data for the ${}^{118}\text{Sn}({}^6\text{Li}, \alpha X)$ reaction are available in Ref. [27] at energies between 18 and 24 MeV. The optical model parameterizations of Refs. [26] and [21] are used for the $\alpha-{}^{118}\text{Sn}$ and $d-{}^{118}\text{Sn}$ systems. For the NEB calculations, the optical potential

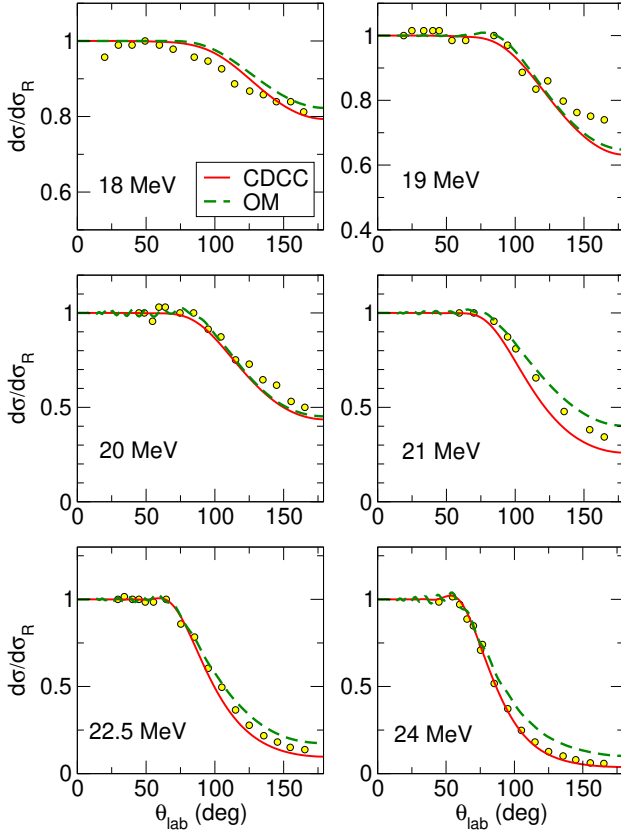


FIG. 5. (Color online) Elastic scattering of ${}^6\text{Li}+{}^{118}\text{Sn}$ at different incident energies. The solid and dashed lines are, respectively, the CDCC calculation and the optical model calculation with the optical potential from [27]. Experimental data are from Ref. [27].

of ${}^6\text{Li}+{}^{118}\text{Sn}$ is taken from Ref. [27].

In Fig. 5 we compare the elastic data with the CDCC (solid lines) and optical model (dashed lines) calculations. Overall, both types of calculations reproduce well the data, with some discrepancy observed at 18 and 21 MeV.

Figure 6 shows the comparison of the calculated and experimental angular distributions of α particles produced in this reaction, for several incident energies. Again, the NEB part (dotted lines) accounts for most of the inclusive breakup cross section and the EBU (dashed lines) becomes the dominant breakup mode for angles smaller than ~ 50 degrees. The summed EBU + NEB result (solid line) reproduces remarkably well the shape and magnitude of the data.

D. ${}^{59}\text{Co}({}^6\text{Li}, \alpha X)$

Experimental data for the α -production channel for the reaction ${}^6\text{Li}+{}^{59}\text{Co}$ have been reported by Souza *et al.* [29] at $E_{\text{lab}} = 21.5$ MeV, which is above the Coulomb barrier ($V_B = 12$ MeV).

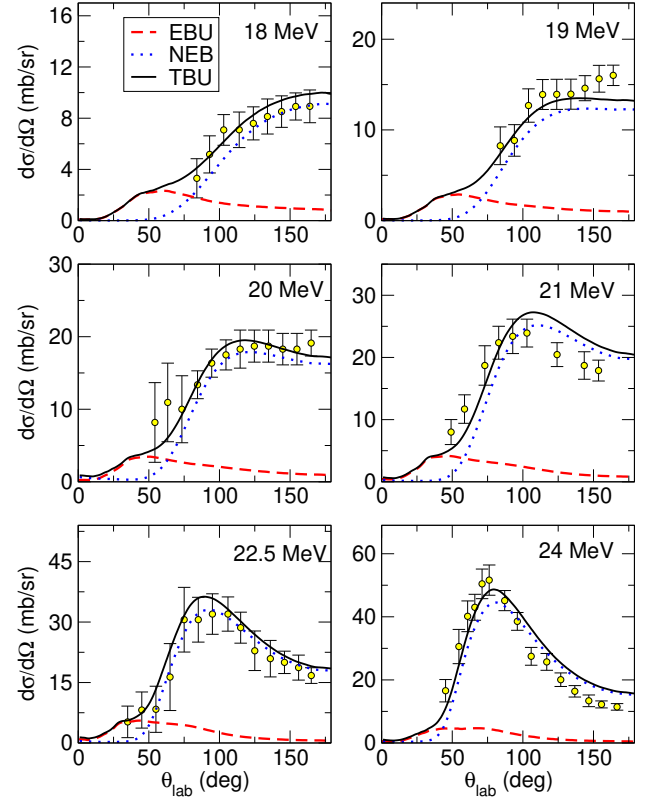


FIG. 6. (Color online) Angular distribution of α particles produced in the reaction ${}^6\text{Li}+{}^{118}\text{Sn}$ at the incident energies indicated by the labels. The dotted, dashed and solid lines correspond to the NEB (IAV model), EBU (CDCC) and their sum (TBU), respectively. Experimental data are from Ref. [27].

Elastic data are available at the somewhat smaller energy $E_{\text{lab}} = 18$ MeV [28] so we first compare these data with the optical model and CDCC calculations. For the former, we employed the global optical potential of Cook [23]. For the CDCC calculations, the optical potentials for $\alpha+{}^{59}\text{Co}$ and $d+{}^{59}\text{Co}$ were taken from Refs. [26] and [21], respectively. The results are shown in Fig. 7. It can be seen that both the CDCC and optical model calculations reproduce fairly well the data. We notice that no renormalization of the deuteron potential was required in this case.

The experimental and calculated angular distributions of inclusive α particles are shown in Fig. 8. The NEB is seen to dominate the inclusive α production. It should be noticed that, in this case, the NEB part includes also the transfer populating bound states of the target, which was obtained using the formalism discussed in Sec. III. A more detailed discussion of this contribution is left for Sec. V. The summed cross section, $\text{TBU} = \text{EBU} + \text{NEB}$, reproduces well the shape of the experimental data, although the magnitude is underestimated by $\sim 30\%$ at the maximum. This might indicate the presence of other relevant mechanisms leading to the production of α particles in this reaction, such as the formation of a compound nu-

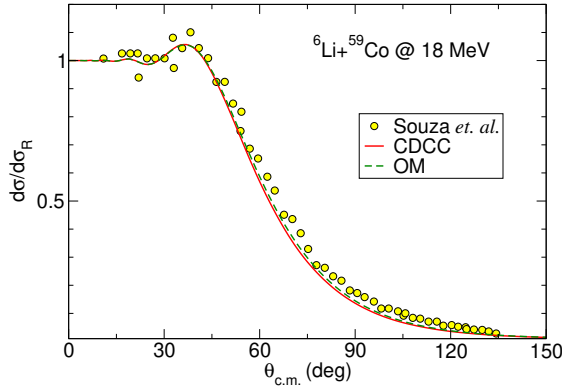


FIG. 7. (Color online) Elastic scattering of ${}^6\text{Li}+{}^{59}\text{Co}$ at an incident energy of 18 MeV. The solid and dashed lines are, respectively, the CDCC calculation and the optical model calculation with the optical potential from [23]. Experimental data are from Ref. [28].

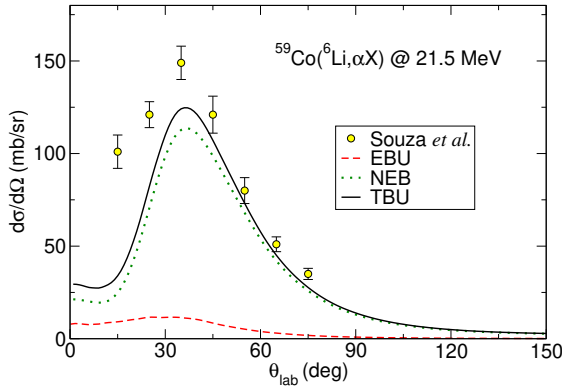


FIG. 8. (Color online) Angular distribution of α particles produced in the reaction ${}^6\text{Li}+{}^{59}\text{Co}$ at an incident energy of 21.5 MeV. The dashed, dotted, and solid lines are, respectively, the EBU (CDCC), NEB (IAV model) and their sum. Experimental data are taken from Ref. [29].

cleus followed by α evaporation. In fact, statistical model calculations performed in Ref. [29] predicted a significant amount of α particles coming from this channel.

The energy spectra for selected α scattering angles are also available for this reaction. These are compared with our calculations in Fig. 9, with each panel corresponding to a given α scattering angle, as indicated by the labels. Except at $\theta_{\text{lab}} = 15^\circ$, the sum of EBU and NEB reproduces the peak of the α production spectra. However, the low-energy tail is clearly underestimated. At these energies, the main contribution of the inclusive α production may arise from compound nucleus followed by evaporation and pre-equilibrium, which are not considered in the present calculations. High energy α particles stem from a deuteron transfer mechanism to the target and are well reproduced by our calculations.

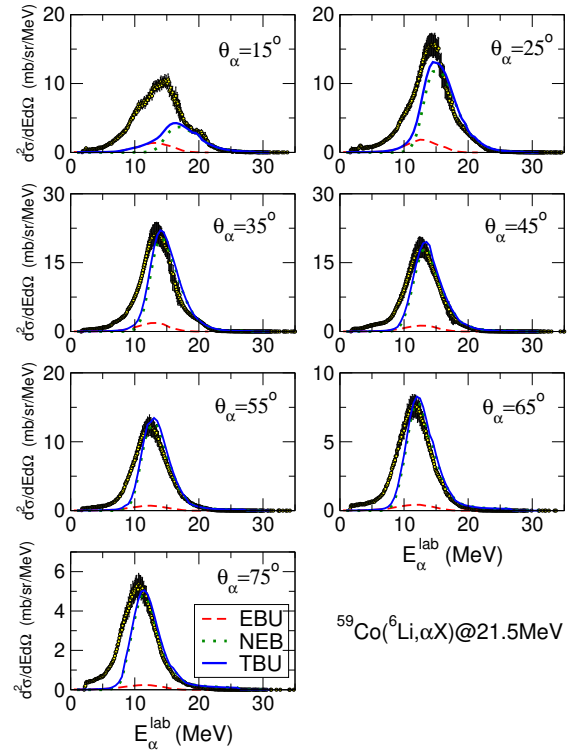


FIG. 9. (Color online) Experimental and calculated inclusive α energy spectra for $E_{\text{lab}} = 21.5$ MeV, at selected scattering angles. The dashed, dotted, and solid lines are respectively the EBU (CDCC), NEB (IAV model) and their sum. Experimental data are taken from Ref. [29].

E. ${}^{58}\text{Ni}({}^6\text{Li}, \alpha X)$

The α production of the ${}^6\text{Li} + {}^{58}\text{Ni}$ reaction at several incident energies between 12 MeV and 20 MeV were measured by Pfeiffer *et al.* [27]. Elastic scattering data, which were also measured, are compared with CDCC and OM calculations in Fig. 10 (note that the angles and cross sections are referred to the laboratory frame, as in the original reference). For the former, we use the same optical potentials as in the nearby ${}^6\text{Li}+{}^{59}\text{Co}$ case. For the OM calculations we use the global OM potential by Cook [23]. Both calculations reproduce fairly well the data, although the CDCC calculations slightly underestimates the data at large angles.

We present now the inclusive alpha cross sections. For the NEB calculation, the ${}^6\text{Li}$ optical potential from Ref. [23] was used. Figure 11 shows the comparison of the calculated and experimental angular distributions of α particles produced in this reaction, for several incident energies. Notice that the NEB (dotted lines) includes also the contribution coming from the transfer to target bound states. Again, the NEB part dominates the inclusive α production. In general, the summed EBU + NEB cross section (solid lines) reproduces fairly well the shape and magnitude of the data. At 16, 18 and 20 MeV some

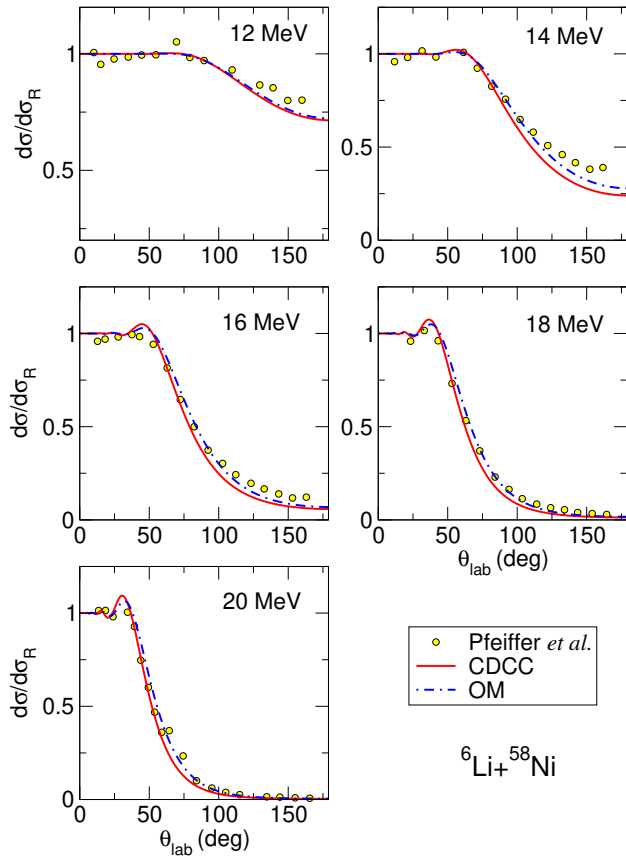


FIG. 10. (Color online) Elastic scattering of ${}^6\text{Li} + {}^{58}\text{Ni}$ at several energies indicated by the labels. The solid and dashed lines are, respectively, the CDCC calculation and the optical model calculation with the optical potential from [27]. Experimental data are from Ref. [27].

underestimation is observed, which might be associated with other α -production channels, as pointed out in the ${}^6\text{Li} + {}^{59}\text{Co}$ case.

From the results presented in the previous sections, we may conclude that the strong α -production channel observed in ${}^6\text{Li}$ experiments originates mostly from non-elastic breakup mechanisms. In all cases analyzed so far, the EBU mode turns out to account for a relatively small fraction of the total inclusive alpha cross section and its contribution is only important for the alpha particles emitted at small angles. We found also an indirect evidence that other alpha production mechanisms, such as fusion, might have some contribution for the lighter targets.

V. TRANSFER CONTENT OF THE NEB CROSS SECTION

The relative importance of the transfer to bound states within the NEB cross section will depend on several parameters, such as the projectile incident energy and the

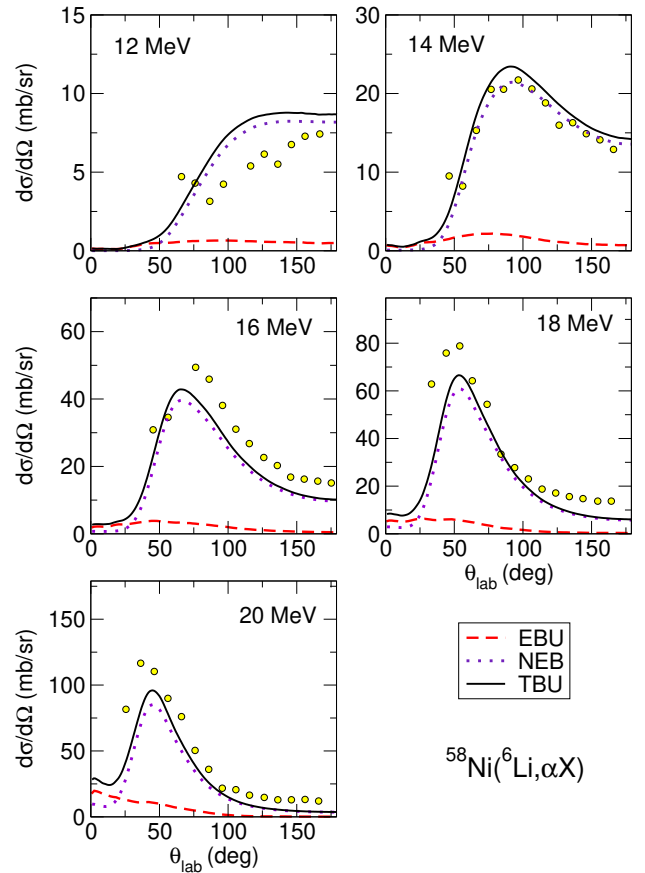


FIG. 11. (Color online) Angular distribution of α particles produced in the reaction ${}^6\text{Li} + {}^{58}\text{Ni}$ at the incident energies indicated by the labels. The dashed, dotted and solid lines are, respectively, the EBU, NEB and their sum. Experimental data are from Ref. [27].

charge of the target nucleus. For heavy targets, the transfer channel is suppressed due to the strong Coulomb interaction between the deuteron and the target, whereas for light targets this channel is expected to play a more important role.

This is illustrated in Fig. 12 for two such cases; the upper panel displays the calculated $({}^6\text{Li}, \alpha)$ NEB cross sections as a function of relative d and ${}^{208}\text{Pb}$ energy in the c.m. frame for the ${}^6\text{Li} + {}^{208}\text{Pb}$ reaction at three different incident energies, 29 MeV, 35 MeV and 39 MeV. The vertical dotted line shows the nominal Coulomb barrier for the d - ${}^{208}\text{Pb}$ system. The bottom panel shows the same observable for the ${}^6\text{Li} + {}^{58}\text{Ni}$ reaction at 12, 16 and 20 MeV. In both cases, it can be seen that the NEB is a *Trojan Horse* type process [30], which means that the ${}^6\text{Li}$ projectile brings the deuteron inside the Coulomb barrier and let it interact with the target nucleus. For the ${}^{208}\text{Pb}$ target, due to the strong Coulomb repulsion, the NEB cross section becomes negligible at low d - ${}^{208}\text{Pb}$ relative energies and this behavior is independent of the incoming ${}^6\text{Li}$ energy. By contrary, for the ${}^{58}\text{Ni}$ target, there is a

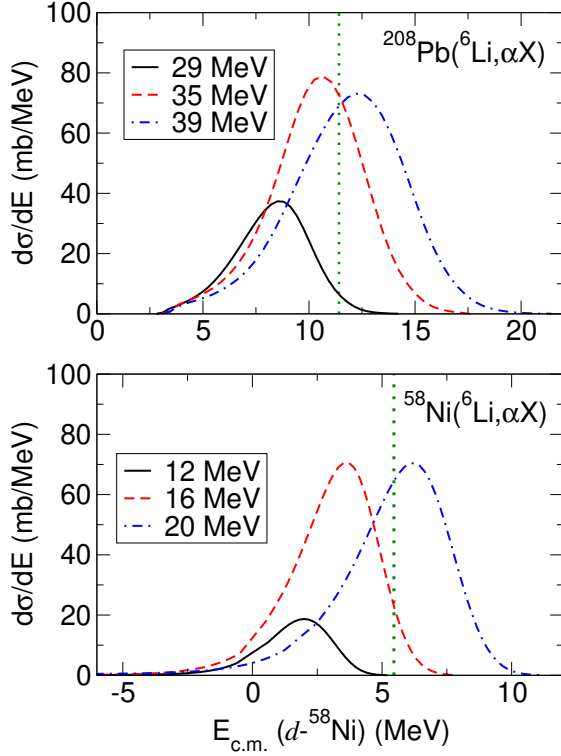


FIG. 12. (Color online) NEB cross section as a function of the d - ^{208}Pb relative energy in the c.m. frame for the reaction $^6\text{Li}+^{208}\text{Pb}$. The solid, dashed and dash-dot lines correspond to the incident energy of 29 MeV, 35 MeV and 39 MeV, respectively. The vertical dotted line indicates the Coulomb barrier of the $d+^{208}\text{Pb}$ system.

low energy tail extending to negative deuteron energies (transfer).

We expect also some correlation between the α -particle angular and energy distribution. This is shown in Fig. 13 in the form of contour plots of double differential cross sections and angle-integrated cross section as a function of the outgoing α energy in the c.m. frame for the reactions (a) $^6\text{Li}+^{208}\text{Pb}$, (b) $^6\text{Li}+^{159}\text{Tb}$, (c) $^6\text{Li}+^{118}\text{Sn}$ and (d) $^6\text{Li}+^{59}\text{Co}$. It can be seen that, the lower outgoing α energies contribute to both forward and backward outgoing angles whereas the higher outgoing α energies only contribute at forward angles. Moreover, when the charge of the target becomes small (^{59}Co), the transfer channel becomes more important.

VI. SYSTEMATICS OF INCLUSIVE α PRODUCTION

Systematic studies of α production yields in ^6Li reactions show an interesting universal behaviour when plotted as a function of the incident energy scaled by the Coulomb barrier energy as reported for instance by Pakou *et al.* [31]. In this section, we will investigate

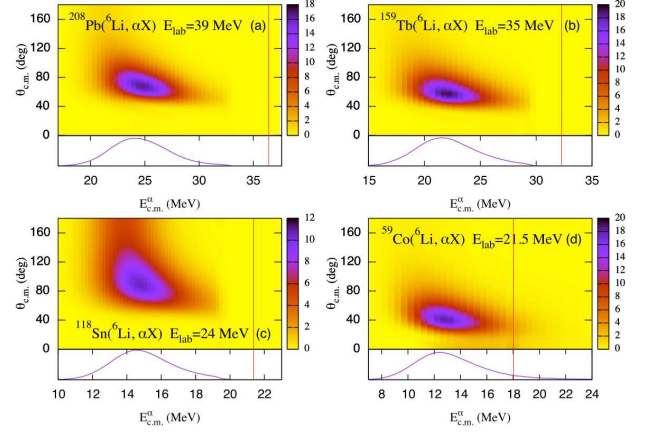


FIG. 13. (Color online) Contour plots for the double differential cross section (upper panels) and the angle-integrated energy differential cross section as a function of the outgoing α energy in the c.m. frame (lower panels) for the reactions: (a) $^6\text{Li}+^{208}\text{Pb}$, (b) $^6\text{Li}+^{159}\text{Tb}$, (c) $^6\text{Li}+^{118}\text{Sn}$ and (d) $^6\text{Li}+^{59}\text{Co}$. The vertical lines indicate the breakup threshold for the d +target system ($E_x = 0$).

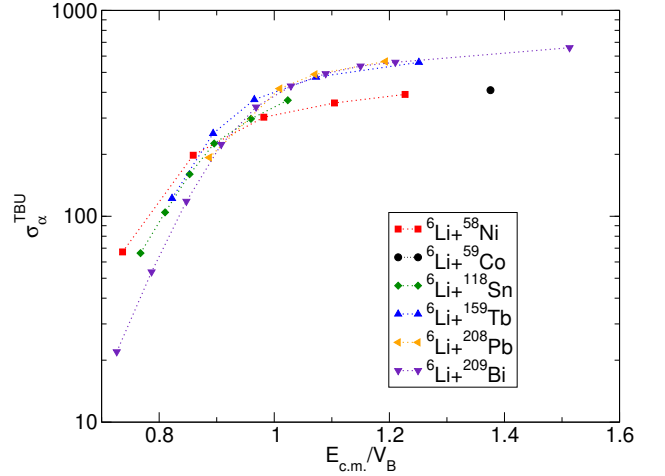


FIG. 14. (Color online) Inclusive breakup α cross sections involving ^6Li projectile with several targets as a function of $E_{c.m.}/V_B$.

whether our calculations exhibit also this universal behaviour. For this study, we have considered the target systems ^{59}Co , ^{118}Sn , ^{159}Tb , ^{208}Pb , which have been analyzed in the preceding sections, and ^{209}Bi , analyzed in Ref. [2]. The results are shown in Fig. 14, where we plot the calculated $\sigma_{\alpha}^{\text{TBU}}$ cross sections as a function of the reduced energy ($E_{c.m.}/V_B$), with V_B the energy of the Coulomb barrier, estimated as $V_B = Z_p Z_t e^2 / (r_B (A_p^{1/3} + A_t^{1/3}))$, where Z_p (Z_t) and A_p (A_t) are the atomic number and atomic mass of the projectile (target), respectively, and $r_B = 1.44$ fm. As expected, the breakup cross section drops quickly as the incident energy decreases below

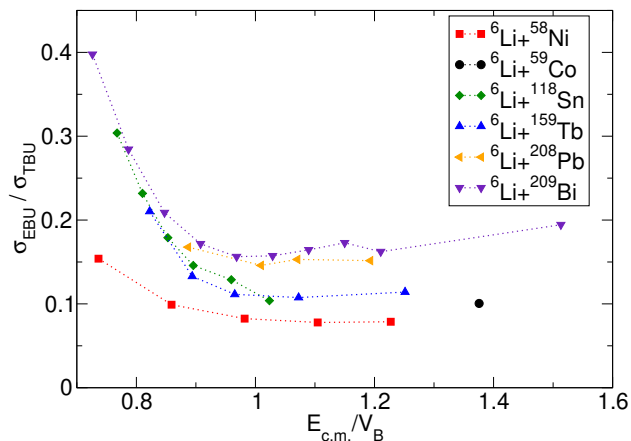


FIG. 15. (Color online) Ratios of calculated EBU over TBU (= EBU + NEB) for different systems. See text for details.

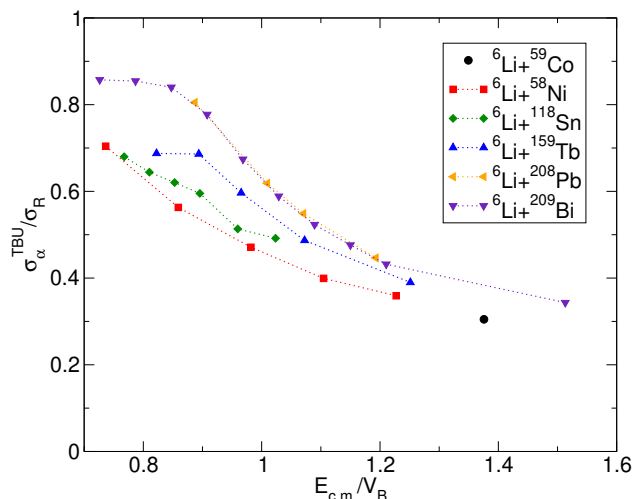


FIG. 16. (Color online) Ratios of calculated TBU (= EBU + NEB) α cross sections over the reaction cross section for the systems and energies analyzed in this work. See text for details.

the barrier. This effect is enhanced for the ^{209}Bi nucleus, possibly due to the larger Coulomb repulsion. Above the barrier, the medium-heavy and heavy targets the inclusive breakup cross sections show a similar trend, but not for the medium mass targets ^{58}Ni and ^{59}Co at larger energies. We recall however that, for these lighter systems, there might be additional contributions from other channels, such as compound nucleus following evaporation, which are not accounted for by the IAV formalism.

We have also studied the relative importance of EBU versus NEB as a function of the incident energy. For that, we display in Fig. 15 the ratio of EBU over TBU (= EBU + NEB) for the analyzed systems. It is seen that, for incident energies below the Coulomb barrier, the elastic breakup cross section becomes comparatively more important as the energy decreases. This can be

attributed to the fact that, below the barrier, the breakup takes place at large projectile-target separations, and the deuteron absorption (responsible for the NEB part) will be less important [4]. By contrast, for energies above the Coulomb barrier, the ratio shows an almost constant behavior. It can also be seen that, while for the heavy mass targets elastic breakup plays an important role in the inclusive α production, especially below the Coulomb barrier, for the medium mass targets elastic breakup is less important and the nonelastic breakup is dominant.

Another relevant question is what fraction of the reaction cross section is exhausted by the α cross section. To address this question, we plot in Fig. 16 the ratio of the calculated TBU and reaction cross sections as a function of the reduced energy $E_{c.m.}/V_B$, for the systems studied in this work. Several interesting features emerge from this plot: (i) first, for all systems analyzed the ratio decreases smoothly as the incident energy increases; (ii) second, the heavier the target nucleus, the larger the ratio. For example, for the ^{208}Pb and ^{209}Bi target nuclei the ratio exceeds 80% at sub-Coulomb energies. Result (i) may be understood as a consequence of the competition with other channels which will open and increase their importance as the incident energy increases, such as other breakup modes not associated with the production of α particles (e.g. $^3\text{H}+^3\text{He}$), target excitation not accompanied by projectile breakup, neutron pickup from the target, etc.

VII. SUMMARY AND CONCLUSIONS

To summarize, we have performed a comprehensive analysis of inclusive breakup cross sections in ^6Li -induced reactions with the aim of understanding the experimentally observed α yields. For that, we have calculated separately the EBU and NEB contributions using the CDCC method (for the EBU part) and the closed-form model proposed by Ichimura, Austern and Vincent IAV theory (for the NEB part). For the latter model, we used the DWBA approximation, including finite-range effects and the remnant term of the transition operator.

Overall, the calculations show a very good agreement with the available data and provide a consistent and neat explanation of the large α yields reported over the years for ^6Li reactions, without the need of evaluating the individual channels contributing to the inclusive cross section. Furthermore, in all cases analyzed, the total α breakup is largely dominated by the NEB part, with the EBU part representing only a small fraction of the total inclusive cross section. This explains why the CDCC calculations tend to largely underpredict the measured α yields. The EBU becomes only dominant at very small angles, or at energies well below the Coulomb barrier. For the heavy target systems, the α singles cross section accounts for a large fraction of the reaction cross section (above 80% at sub-Coulomb energies). For the lighter mass targets, we found that part of the α yields

corresponds to transfer to bound states of the residual nucleus. To account for this contribution, the IAV model has been conveniently extended, following the formalism developed by previous authors [10, 11].

Finally, we have investigated whether our calculations support the observed universal trend of α yields as a function of the reduced incident energy ($E_{c.m.}/V_B$). We find that the computed total breakup cross sections (EBU+NEB) exhibit this trend for the heavy targets, but significant deviations have been found for the light targets. This could indicate that the latter do not obey the universal behavior, but we cannot rule out that the deviations are due to the presence of additional α produc-

tion mechanisms, not included in our calculations. This problem deserves further investigation.

ACKNOWLEDGMENTS

We are grateful to Gregory Potel for his guidance in the extension of the IAV model to negative energies. This work has been partially supported by the Spanish Ministerio de Economía y Competitividad and FEDER funds under project FIS2014-53448-C2-1-P and by the European Union's Horizon 2020 research and innovation program under grant agreement No. 654002.

-
- [1] C. Signorini, A. Edifizi, M. Mazzocco, M. Lunardon, D. Fabris, A. Vitturi, P. Scopel, F. Soramel, L. Stroe, G. Prete, E. Fioretto, M. Cinausero, M. Trotta, A. Brondi, R. Moro, G. La Rana, E. Vardaci, A. Ordine, G. Inglima, M. L. Commara, D. Pierroutsakou, M. Romoli, M. Sandoli, A. Diaz-Torres, I. J. Thompson, and Z. H. Liu, *Phys. Rev. C* **67**, 044607 (2003).
 - [2] J. Lei and A. M. Moro, *Phys. Rev. C* **92**, 044616 (2015).
 - [3] J. Lei and A. M. Moro, *Phys. Rev. C* **92**, 061602(R) (2015).
 - [4] A. M. Moro and J. Lei, *Few-Body Systems* **57**, 319 (2016).
 - [5] B. V. Carlson, R. Capote, and M. Sin, *Few-Body Systems* **57**, 307 (2016).
 - [6] G. Potel, F. M. Nunes, and I. J. Thompson, *Phys. Rev. C* **92**, 034611 (2015).
 - [7] H. Feshbach, *Annals of Physics* **19**, 287 (1962).
 - [8] M. Ichimura, N. Austern, and C. M. Vincent, *Phys. Rev. C* **32**, 431 (1985).
 - [9] N. Austern, Y. Iseri, M. Kamimura, M. Kawai, G. Rawitscher, and M. Yahiro, *Phys. Rep.* **154**, 125 (1987).
 - [10] T. Udagawa, Y. J. Lee, and T. Tamura, *Phys. Rev. C* **39**, 47 (1989).
 - [11] G. Potel, F. M. Nunes, and I. J. Thompson, in *Proceedings, 14th International Conference on Nuclear Reaction* (2015) pp. 155–162, arXiv:1510.02727 [nucl-th].
 - [12] C. Mahaux and R. Sartor, *Physical review letters* **57**, 3015 (1986).
 - [13] C. Mahaux and R. Sartor, in *Advances in nuclear physics* (Springer, 1991) pp. 1–223.
 - [14] W. Dickhoff, R. Charity, and M. Mahzoon, arXiv preprint arXiv:1606.08822 (2016).
 - [15] I. J. Thompson, *Comp. Phys. Rep.* **7**, 167 (1988).
 - [16] S. Watanabe, T. Matsumoto, K. Minomo, K. Ogata, and M. Yahiro, *Phys. Rev. C* **86**, 031601 (2012).
 - [17] Y. Hirabayashi and Y. Sakuragi, *Phys. Lett. B* **258**, 11 (1991).
 - [18] H. Nishioka, J. Tostevin, R. Johnson, and K.-I. Kubo, *Nucl. Phys. A* **415**, 230 (1984).
 - [19] C. Signorini, M. Mazzocco, G. F. Prete, F. Soramel, L. Stroe, A. Andrichetto, I. J. Thompson, A. Vitturi, A. Brondi, M. Cinausero, D. Fabris, E. Fioretto, N. Gelli, J. Y. Guo, G. La Rana, Z. H. Liu, F. Lucarelli, R. Moro, G. Nebbia, M. Trotta, E. Vardaci, and G. Viesti, *Eur. Phys. J. A* **10**, 249 (2001).
 - [20] G. R. Kelly, N. J. Davis, R. P. Ward, B. R. Fulton, G. Tungate, N. Keeley, K. Rusek, E. E. Bartosz, P. D. Cathers, D. D. Caussyn, T. L. Drummer, and K. W. Kemper, *Phys. Rev. C* **63**, 024601 (2000).
 - [21] Y. Han, Y. Shi, and Q. Shen, *Phys. Rev. C* **74**, 044615 (2006).
 - [22] A. R. Barnett and J. S. Lilley, *Phys. Rev. C* **9**, 2010 (1974).
 - [23] J. Cook, *Nucl. Phys. A* **388**, 153 (1982).
 - [24] M. K. Pradhan, A. Mukherjee, S. Roy, P. Basu, A. Goswami, R. Kshetri, R. Palit, V. V. Parkar, M. Ray, M. Saha Sarkar, and S. Santra, *Phys. Rev. C* **88**, 064603 (2013).
 - [25] J. M. Figueira, J. O. F. Niello, A. Arazi, O. A. Capurro, P. Carnelli, L. Fimiani, G. V. Martí, D. M. Heimann, A. E. Negri, A. J. Pacheco, J. Lubian, D. S. Monteiro, *Adv. Phys. C: Complex Phys. Rev. C* **81**, 024613 (2015).
 - [26] J. R. Huizenga and G. Igo, *Nucl. Phys.* **29**, 462 (1962).
 - [27] K. Pfeiffer, E. Speth, and K. Bethge, *Nucl. Phys. A* **206**, 545 (1973).
 - [28] F. A. Souza, L. A. S. Leal, N. Carlin, M. G. Munhoz, R. L. Neto, M. M. d. Moura, A. A. P. Suaide, E. M. Szanto, A. S. d. Toledo, and J. Takahashi, *Phys. Rev. C* **75**, 044601 (2007).
 - [29] F. Souza *et al.*, *Nucl. Phys. A* **821**, 36 (2009).
 - [30] G. Baur, *Physics Letters B* **178**, 135 (1986).
 - [31] A. Pakou, N. Alamanos, A. Gillibert, M. Kokkoris, S. Kossionides, A. Lagoyannis, N. G. Nicolis, C. Papachristodoulou, D. Patiris, D. Pierroutsakou, E. C. Polacco, and K. Rusek, *Phys. Rev. Lett.* **90**, 202701 (2003).